Published in final edited form as:

Oncogene. 2021 April ; 40(17): 3118–3135. doi:10.1038/s41388-021-01771-z.

Loss of activating transcription factor 3 prevents KRAS-mediated pancreatic cancer

Nawab Azizi[1,2], **Jelena Toma**[1,2,3], **Mickenzie Martin**[1,2,4], **Muhammad Faran Khalid**[1,5], **Fatemeh Mousavi**[1,2], **Phyo Wei Win**[1,5], **Maria Teresa Borrello**[6], **Nina Steele**[7], **Jiaqi Shi**[7], **Marina Pasca di Magliano**[8], **Christopher L. Pin**[1,2,3,5]

[1]Children's Health Research Institute, London, ON, Canada

[2]Department of Physiology and Pharmacology, University of Western Ontario, London, ON, Canada

[3]Department of Oncology, University of Western Ontario, London, ON, Canada

[4]Department of Biology, University of Western Ontario, London, ON, Canada

[5]Department of Paediatrics, University of Western Ontario, London, ON, Canada

[6]Centre for Cancer Research Marseille, INSERM U1068, CNRS UMR 7258, Aix-Marseille Université and Institut Paoli-Calmettes, Marseille, France

[7]Department of Pathology, University of Michigan, Ann Arbor, MI, USA

[8]Department of Surgery, University of Michigan, Ann Arbor, MI, USA

Abstract

The unfolded protein response (UPR) is activated in pancreatic pathologies and suggested as a target for therapeutic intervention. In this study, we examined activating transcription factor 3 (ATF3), a mediator of the UPR that promotes acinar-to-ductal metaplasia (ADM) in response to pancreatic injury. Since ADM is an initial step in the progression to pancreatic ductal adenocarcinoma (PDAC), we hypothesized that ATF3 is required for initiation and progression of PDAC. We generated mice carrying a germline mutation of *Atf3* (*Atf3*$^{-/-}$) combined with acinar-specific induction of oncogenic KRAS (*Ptf1a*$^{creERT/+}$*Kras*$^{G12D/+}$). *Atf3*$^{-/-}$ mice with (termed *APK*) and without KRAS^{G12D} were exposed to cerulein-induced pancreatitis. In response to recurrent pancreatitis, *Atf3*$^{-/-}$ mice showed decreased ADM and enhanced regeneration based on morphological and biochemical analysis. Similarly, an absence of ATF3 reduced spontaneous pancreatic intraepithelial neoplasia (PanIN) formation and PDAC in *Ptf1a*$^{creERT/+}$*Kras*$^{G12D/+}$ mice. In response to injury, KRAS^{G12D} bypassed the requirement for ATF3 with a dramatic loss in acinar tissue and PanIN formation observed regardless of ATF3 status. Compared to

Christopher L. Pin, cpin@uwo.ca.

Compliance with ethical standards

Conflict of interest The authors declare no competing interests.

Ethical approval All animal experiments were performed according to regulations established by the Animal Care and Use Committee at Western University (protocol #2017-001).

Supplementary information The online version contains supplementary material available at https://doi.org/10.1038/s41388-021-01771-z.

Ptf1a$^{creERT/+}$*Kras*$^{G12D/+}$ mice, *APK* mice exhibited a significant decrease in pancreatic and total body weight, did not progress through to PDAC, and showed altered pancreatic fibrosis and immune cell infiltration. These findings suggest a complex, multifaceted role for ATF3 in pancreatic cancer pathology.

Introduction

The unfolded protein response (UPR) is a critical pathway protecting cells from a variety of harmful stresses that promote improper protein folding or processing [1, 2]. In response to accumulation of misfolded proteins, the UPR is activated to reduce protein load through a general decrease in protein translation, activation of ER-associated degradation, and increased expression of protein chaperones [1–3]. Over the last decade, the UPR has been implicated in a variety of human pathologies, including breast [4], lung [5], and colorectal cancer [6, 7]. In the pancreas, the UPR plays important roles in both physiological and pathological processes. More recently, the UPR has been suggested as a mediator and potential therapeutic target for pancreatic ductal adenocarcinoma (PDAC [8, 9]). PDAC is currently the third leading cause of cancer-related deaths, with a dismal 5-year survival rate of ~9%. While constitutive activation of KRAS is an initiating event in PDAC, targeting this pathway has been futile to date, suggesting alternative targets need to be identified. Studies with pancreatic cancer cell lines indicate that targeting the UPR may be beneficial [8, 10]. However, the mechanism(s) of action of the UPR in cancer initiation and progression have been elusive. This is likely due to the numerous levels of regulation that exist for the UPR both before and after activation.

Within acinar cells, mediators of the UPR play a pivotal role in normal physiology, preventing accumulation of misfolded proteins in the ER lumen and maintaining protein homeostasis [11]. The UPR consists of three signaling branches—PKR-like ER kinase (PERK [12]), inositol requiring enzyme 1 (IRE1 [13]), and activating transcription factor 6 (ATF6 [14]). These ER-membrane-associated proteins are triggered through dissociation of GRP78/BiP in response to accumulation of misfolded protein [15]. Activation of PERK leads to phosphorylation of eIF2α that then leads to global inhibition of mRNA translation [12]. An important mediator of PERK signaling is ATF4, which is transcribed, but in the absence of stress, not translated as a functional protein [16]. Upon stress, *Atf4* avoids translational inhibition and activates genes that regulate protein folding, degradation, and cell survival [17, 18]. PERK signaling also activates *Atf3* gene expression [19].

Likely due to the high protein turnover rate in acinar cells [13], deletion of genes encoding several important mediators of the UPR, including IRE1 [13], PERK [20], and ATF4 [20], all result in pancreatic pathology highlighting their importance to acinar cell physiology. To understand the pathological requirement of the UPR, we have focused on ATF3, which is not expressed in the pancreas until induced by injury, such as observed in pancreatitis [21]. Previous work from our laboratory and others showed that ATF3 expression is rapidly induced in acinar cells by experimental forms of pancreatitis [22, 23]. In other organs or pathologies, ATF3 affects signaling pathways and cellular processes that are observed in pancreatitis and PDAC. ATF3 interacts with SMAD and MAPK signaling pathways [24] to

relieve stress through DNA damage repair and cell cycle regulation [25], binds NF-κB and represses the expression of cytokines such as TLR-4 and IL-6 [26, 27], and is vital for neutrophil migration to areas of injury in lung tissue [28]. In the skin, ATF3 is critical for negatively regulating cancer-associated fibroblasts to prevent the excessive deposition of extracellular matrix (ECM) proteins that would otherwise promote carcinogenesis [29].

While roles for ATF3 has been identified in several cancers, these are cell and cancer-type dependent [6, 7, 30]. Conflicting roles for ATF3 have been reported for metastatic prostate cancer [31]. In breast cancer, high levels of ATF3 are associated with increased chemoresistance [4] and promote tumor development and metastasis [32]. Alternatively, in colon and colorectal cancers, ATF3 overexpression reduces cell survival by exerting anti-tumorigenic effects [33, 34]. ATF3's role in pancreatic cancer has not been examined to date.

Loss of the acinar cell phenotype or acinar-to-ductal metaplasia (ADM) is an early event in chronic pancreatitis and PDAC. Our laboratory showed that ATF3 is required for ADM during acute injury [22] by activating Sry-related high-mobility group box 9 (*Sox9*) and repressing *Mist1*, which maintains the mature acinar cell phenotype [35]. SOX9 and MIST1 are important regulators of ADM, required for [36] or limiting [37] PDAC progression through ADM/pancreatic intraepithelial neoplasia (PanIN) formation, respectively.

These studies suggest that ATF3 may have an early role in progression of PDAC, possibly through regulation of key transcription factors involved in the ADM process. However, while recurrent or chronic forms of pancreatitis are a significant risk factor for PDAC, acute pancreatitis is a poor predictor of PDAC [38]. Therefore, in this study we investigated whether ATF3 is required for ADM in recurrent injury and whether oncogenic KRAS could override this requirement. Our findings suggest that ADM can occur in KRAS-mediated PDAC, but ATF3 is required for progression and maintenance of high-grade PanIN lesions and PDAC. In addition, it appears that ATF3 may affect multiple cell types involved in PDAC.

Results

ATF3 is required for activating the transcriptional program for ADM during recurrent pancreatic injury

To determine if ATF3 is critical for the loss of the acinar cell phenotype during recurrent pancreatic injury, congenic wild-type (WT) and $Atf3^{-/-}$ mice were subjected to recurrent cerulein-induced pancreatitis (rCIP) for 14 days (Supplementary Fig. S1A). Since ATF3 expression is observed up to 28 days after rCIP [22], pancreatic tissue was collected 1 and 7 days following cessation of cerulein to assess the extent of injury and regeneration, respectively. No gross morphological differences were observed between WT and $Atf3^{-/-}$ mice during rCIP. Both cerulein-treated groups showed significant weight loss compared to saline-treated groups, but all groups showed increased weight gain following cessation of the injections (Supplementary Fig. S1B). One day following treatment, both cerulein-treated groups showed a significant decrease in pancreas/body weight ratio relative to saline groups (Fig. 1A), with no difference between WT and $Atf3^{-/-}$ mice. Both genotypes acquired a

similar extent of damage (Fig. 1B), including loss of acinar tissue based on amylase immunohistochemistry (IHC) (Fig. 1C), western blot analysis (Fig. 1D), serum amylase levels (Supplementary Fig. S1C), and fibrosis (Supplementary Fig. S2). While morphological staining indicated similar accumulation of duct-like structures in cerulein-treated WT and *Atf3*$^{-/-}$ tissue (Fig. 2A), IHC for CK19 expression was less extensive in *Atf3*$^{-/-}$ tissue (Fig. 2B). Quantification of the extent of CK19 accumulation confirmed a reduction in the total amount of CK19+ cells in *Atf3*$^{-/-}$ tissue compared to WT mice (Fig. 2C).

Seven days after rCIP, the differences between WT and *Atf3*$^{-/-}$ pancreatic tissue were striking. Pancreas to body weight ratio of cerulein-treated *Atf3*$^{-/-}$ mice was similar to saline-treated mice, while cerulein-treated WT mice still had significantly smaller pancreata relative to all other groups (Fig. 1A). Histological analysis showed almost a complete recovery of acinar tissue in cerulein-treated *Atf3*$^{-/-}$ mice while WT mice retained areas of damage (Fig. 1B). Acinar tissue was restored more quickly based on histology (Figs. 1B and 2A and Supplementary Fig. S2A), amylase accumulation (Fig. 1C–E), and CK19 accumulation (Fig. 2B, C). While serum amylase levels were slightly higher in cerulein-treated *Atf3*$^{-/-}$ mice (Supplementary Fig. S1C), possibly reflective of the restoration of acinar tissue, this difference was not significant. Analysis of fibrosis showed no difference between WT and *Atf3*$^{-/-}$ mice, with overall fibrosis reduced by day 7 compared to day 1 in both genotypes (Supplementary Fig. S2).

Our previous work indicated that ATF3 directly regulated expression of transcription factors involved in ADM [22]. Immunofluorescence (IF) for SOX9, which is required for ADM [36, 39], showed limited expression in saline-treated animals, localizing specifically to ductal epithelial cells. As previously reported, SOX9 expression was observed in acinar cells and ADM structures 1 and 7 days following rCIP in WT mice (Fig. 3A, B). This finding was confirmed by western blotting (Supplementary Fig. S3A). Conversely, SOX9 expression was observed only sporadically in cerulein-treated *Atf3*$^{-/-}$ tissue (Fig. 3A, B) with no increase observed by western blot analysis (Supplementary Fig. S3A). Similar analysis for PDX1 showed increased accumulation in ADM structures in cerulein-treated WT pancreatic tissue, while PDX1 expression was greatly reduced in both intensity (Supplementary Fig. S3B) and frequency in cerulein-treated *Atf3*$^{-/-}$ pancreas tissue (Supplementary Fig. S3C).

We next examined MIST1, which is required for establishing the mature acinar cell phenotype [40]. As previously reported [22], MIST1 expression is significantly reduced in WT acinar cells 1 day following cessation of cerulein treatment (Fig. 3C, D). Seven days after treatment, MIST1 expression returned to control levels. Conversely, this temporal decrease in MIST1 expression was not observed in cerulein-treated *Atf3*$^{-/-}$ tissue (Fig. 3C, D). Given the importance of epidermal growth factor (EGF) signaling to ADM, the expression of *Egfr* and *Mek1* was examined to determine if the absence of ATF3 affected this pathway (Supplementary Fig. S4). qRT-PCR revealed increased *Egfr* and *Mek1* expression 4 h after the initial cerulein injection in WT tissue consistent with an activation of EGF signaling before any evidence of ADM. This increased expression was muted (*Egfr*) or absent (*Mek1*) in *Atf3*$^{-/-}$ tissue (Supplementary Fig. S4A). Seventy-two hours after initial cerulein injection, no difference in *Egfr* and *Mek1* expression was observed in *Atf3*$^{-/-}$

pancreas, while elevated expression of both genes was found in WT tissue (Supplementary Fig. S4B). These findings suggest that ATF3 regulates multiple mediators of the ADM process. Combined, these data suggest that *Atf3*$^{-/-}$ mice recover more quickly from rCIP, possibly through limiting activation of a more progenitor-like state in response to injury.

Absence of ATF3 reduces spontaneous PanIN progression following KRAS^{G12D} activation

While ATF3 was required for activating the ADM transcriptional program in response to injury, it is possible that oncogenic KRAS can bypass this requirement. Therefore, *Atf3*$^{-/-}$ mice were mated to mice allowing inducible activation of oncogenic KRAS (KRAS^{G12D}). Recombination was limited to acinar cells by targeting a creERT to the *Ptf1a* gene [41]. These mice contained a *ROSA26* reporter gene (*R26r-YFP*) allowing analysis of cre-mediated recombination. Two- to four-month-old mice with (*Atf3*$^{+/+}$ or *Atf3*$^{+/-}$ *Ptf1a*$^{creERT/+}$ *Kras*$^{LSL\text{-}G12D/+}$; referred to as *Ptf1a*$^{creERT/+}$ *Kras*$^{G12D/+}$) or without ATF3 (*Atf3*$^{-/-}$ *Ptf1a*$^{creERT/+}$ *Kras*$^{LSL\text{-}G12D/+}$; referred to as *APK*) were treated with tamoxifen for 5 days (Supplementary Fig. S5A). *Ptf1a*$^{creERT/+}$ (essentially WT mice) and *Atf3*$^{-/-}$ *Ptf1a*$^{creERT/+}$ mice were included as controls. This resulted in >95% acinar-specific recombination in *Ptf1a*$^{creERT/+}$ lines with no observable recombination in duct or islet tissue based on activation of the *ROSA26r-LSL-YFP* locus (Supplementary Fig. S5B). One cohort of mice was followed for 13 weeks to determine if spontaneous ADM and PanIN lesions were affected by the absence of ATF3 (Supplementary Fig. S5A). All groups showed a decrease in weight in response to tamoxifen, which was regained over the course of the experiment (Supplementary Fig. S5D, E). Upon dissection, 2/5 *Ptf1a*$^{creERT/+}$ *Kras*$^{G12D/+}$ mice contained pancreata with some fibrotic masses observed at the gross morphological level (data not shown). Pancreatic weight as a percentage of total body weight was increased in *Ptf1a*$^{creERT/+}$ *Kras*$^{G12D/+}$ mice relative to all other genotypes (Fig. 4A). H&E analysis confirmed significant disruptions to pancreatic architecture, including loss of acini, extensive PanIN lesions, inflammation, and fibrosis in 2/5 *Ptf1a*$^{creERT/+}$ *Kras*$^{G12D/+}$ mice (Fig. 4B). In the remaining three *Ptf1a*$^{creERT/+}$ *Kras*$^{G12D/+}$ mice, areas of ADM and early PanIN lesions were readily observed (Fig. 4B and Supplementary Fig. S6) and were all derived from recombined acinar tissue based on *yellow fluorescent protein* (YFP) expression (Supplementary Fig. S5C). IHC for ATF3 shows moderate increases in ATF3 expression in response to oncogenic KRAS (Supplementary Fig. S7A), although not nearly as high as that observed early during cerulein exposure. Indeed, western blot analysis did not detect ATF3 accumulation, likely due to the low level of expression. However, single-cell RNA-seq of tumors derived from PKC mice confirmed that ATF3 expression is found in epithelial, myeloid, and fibroblast cells, while acinar cells show limited ATF3 expression (Supplementary Fig. S7B). IF revealed SOX9 expression within the ADM and PanIN lesions observed in *Ptf1a*$^{creERT/+}$ *Kras*$^{G12D/+}$ tissue (Fig. 4D). Conversely, *APK* mice showed only sporadic ADM/PanIN lesions (Fig. 4B and Supplementary Fig. S6) with minimal to no SOX9 expression (Fig. 4D) and no PanIN2 or PanIN3 lesions. The ADM and PanIN lesions that do appear in *APK* mice are positive for CK19 (Fig. 4E), with some lesions staining for PAS (Supplementary Fig. 6B) and Alcian blue (Fig. 4E), although the staining was not as intense or as widespread as observed in *Ptf1a*$^{creERT/+}$ *Kras*$^{G12D/+}$ tissue. In addition, IHC shows that the lesions that appear in both lines are positive for p-ERK, although nuclear localization was only readily apparent in *Ptf1a*$^{creERT/+}$ *Kras*$^{G12D/+}$ lesions (Fig. 4E). These

results indicated that the absence of ATF3 reduces spontaneous KRAS^{G12D}-mediated PanIN formation.

Oncogenic KRAS bypasses the requirement of *ATF3* for ADM following injury

Next, we exposed *Ptf1a$^{creERT/+}$Kras$^{G12D/+}$* and *APK* mice to a two-day regime of acute cerulein treatment 7 days after tamoxifen treatment and examined pancreatic tissue 2 and 5 weeks after cerulein treatment (Supplementary Fig. S5A). During tamoxifen treatment and acute CIP, mice were weighed daily. All saline-treated mice, regardless of ATF3 expression or oncogenic KRAS activity gained body weight over the experimental time period (Supplementary Fig. S7A). CIP-treated *Ptf1a$^{creERT/+}$Kras$^{G12D/+}$* mice showed reduced body weight starting 43 days after tamoxifen treatment compared to *Ptf1a$^{creERT/+}$* and *Atf3$^{-/-}$ Ptf1a$^{CreERT/+}$* mice, while *APK* mice treated with cerulein had significantly reduced body weight compared to all other genotypes 31 days into treatment (Supplementary Fig. S8B). Both *Ptf1a$^{creERT/+}$Kras$^{G12D/+}$* (3/22 mice) and *APK* lines (1/14 mice) exhibited some mortality during the 5-week experimental time point. Upon dissection, *APK* mice appeared much smaller than other groups with negligible abdominal wall muscle observed in most of these mice (data not shown). *APK* mice also had significantly smaller pancreata at both time points examined relative to other genotypes (Supplementary Fig. S8C, D). Conversely, cerulean-treated *Ptf1a$^{creERT/+}$Kras$^{G12D/+}$* mice had significantly increased pancreatic weight relative to body weight (Supplementary Fig. S8D) compared to all other groups 2 weeks post treatment, with multiple fibrotic nodules visible (Supplementary Fig. S7C). By 5 weeks, the difference in pancreatic/body weight was no longer apparent in *Ptf1a$^{creERT/+}$Kras$^{G12D/+}$* mice, even though nodules were still present. Histological analysis of pancreatic tissue indicated complete loss of acinar tissue and development of ADM and PanIN lesions within 2 weeks of inducing CIP in *APK* and *Ptf1a$^{creERT/+}$Kras$^{G12D/+}$* pancreatic tissues (Fig. 5A). The loss of acinar tissue was confirmed by a complete absence of amylase accumulation based on western blot analysis (Fig. 6A, B).

Cursory H&E analysis suggests ATF3 is not required for KRAS^{G12D}-mediated PDAC progression. Saline- and cerulein-treated control *Ptf1a$^{creERT/+}$* and *Atf3$^{-/-}$ Ptf1a$^{creERT/+}$* tissue showed no damage either 2 or 5 weeks after treatment (Supplementary Fig. S9A and Fig. 5A). To determine if the pathological phenotype was the same between *APK* and *Ptf1a$^{creERT/+}$Kras$^{G12D/+}$* mice, tissue was assessed based on the highest grade lesion present per tissue area (Table 1). As suggested from 13-week analysis, saline-treated *APK* and *Ptf1a$^{creERT/+}$Kras$^{G12D/+}$* mice showed some pre-neoplastic lesions (Supplementary Fig. S9A, B and Table 1). Upon CIP treatment, *APK* and *Ptf1a$^{creERT/+}$Kras$^{G12D/+}$* mice treated with cerulein showed high-grade PanIN3 lesions 2 two weeks after CIP (Fig. 5A and Table 1). However, by week 5, *APK* tissue showed predominately low-grade PanIN1 and 2 lesions (only 2/8 progress to PanIN3) compared to predominantly high-grade PanIN3 and PDAC lesions observed in *Ptf1a$^{creERT/+}$Kras$^{G12D/+}$* tissue (5/7 progress to PanIN3/PDAC; Table 1). In no instance was PDAC observed in *APK* tissue suggesting the pre-cancerous lesions did not progress in the absence of ATF3. The decrease in progressive PanIN lesions in *APK* mice was also reflected by reduced accumulation of CK19+ ducts in *APK* tissue compared to *Ptf1a$^{creERT/+}$Kras$^{G12D/+}$* mice (Supplementary Fig. S9C, D). Alcian blue stain, which identifies mucin and suggests metaplastic PanIN lesions, was significantly reduced in *APK*

tissue relative to *Ptf1a*$^{creERT/+}$ *Kras*$^{G12D/+}$ tissue (Fig. 5C, D). Finally, epithelial cell proliferation in PanINs was examined by Ki-67 fluorescence. Ki67+ cells were reduced at 2 weeks and completely absent at 5 weeks in *APK* lesions relative to *Ptf1a*$^{creERT/+}$*Kras*$^{G12D/+}$ tissue (Fig. 5E, F). Therefore, while overall histology was similar between *APK* and *Ptf1a*$^{creERT/+}$*Kras*$^{G12D/+}$ tissue, multiple analyses suggest that the absence of ATF3 affects KRAS^{G12D}-mediated progression to PDAC.

We next examined if the molecular profile for ADM progression was present in *APK* mice. Both transcriptional (SOX9) and signaling mediators (phosphorylated MAPK1/2) of ADM (Fig. 6) were examined. IF for SOX9 showed equivalent numbers of SOX9+ cells 2 weeks after CIP in *Ptf1a*$^{creERT/+}$*Kras*$^{G12D/+}$ and *APK* tissue (Fig. 6D), but with significantly lower SOX9 accumulation in *APK* tissue based on western blot analysis (Fig. 6A, C; SOX9 accumulation is 7.99 ± 1.24-fold higher in *Ptf1a*$^{creERT/+}$*Kras*$^{LSL\text{-}G12D/+}$ extracts compared to *APK*). By 5 weeks post cerulein, both the number of SOX9+ cells (Fig. 6D) and level of SOX9 accumulation were reduced in *APK* mice (Fig. 6C; 2.58 ± 1.41-fold higher in *Ptf1a*$^{creERT/+}$*Kras*$^{LSL\text{-}G12D/+}$ extracts). The decreased expression of the ADM-promoting SOX9 was consistent with decreased activation of MAPK signaling in *APK* tissue based on western blot analysis for p-ERK both 2 (2.21 ± 0.66-fold less p-ERK) and 5 weeks (2.42 ± 0.25-fold less p-ERK) after injury compared to *Ptf1a*$^{creERT/+}$*Kras*$^{G12D/+}$ tissue (Fig. 6A, E), as well as by IHC at 2 weeks post CIP (Fig. 6F and Supplementary Fig. S9E). In *Ptf1a*$^{creERT/+}$*Kras*$^{G12D/+}$ tissue, p-ERK shows predominant localization to PanIN and ADM nuclei, while in *APK* tissue, p-ERK seems more diffuse. In addition, a few cells within the stroma appear to be p-ERK positive only in *APK* mice.

Examination of PERK signaling showed that activation of KRAS had no significant effect on ATF4 or CHOP expression in saline-treated mice. Increased BiP/GRP78 expression was observed only when KRAS^{G12D} was combined with a loss of *Atf3* ($p < 0.005$; WT saline vs. *APK* saline; Supplementary Fig. S10A, B). However, upon cerulein administration, BiP/GRP78 expression was significantly reduced in both *Ptf1a*$^{creERT/+}$*Kras*$^{G12D/+}$ and *APK* tissue ($p < 0.01$) relative to saline-treated mice or CIP-treated WT and *Atf3*$^{-/-}$*Ptf1a*$^{CreERT/+}$ mice. Decreased BiP/GRP78 could lead to increased activation of all UPR pathways, and increased ATF3 (Supplementary Fig. S7) expression supports elevated PERK activation. However, while CHOP expression appears to increase upon CIP treatment only in *Ptf1a*$^{creERT/+}$ *Kras*$^{G12D/+}$ and *APK* mice, it was not significantly different in either case ($p = 0.069$ and $p = 0.156$ relative to saline, respectively). In addition, ATF4 accumulation appeared to decrease in response to KRAS^{G12D} expression, only approaching significance when coupled with the absence of *Atf3* ($p = 0.057$, *APK* saline vs. *APK* CIP). This analysis suggests that ATF3's primary effects on KRAS^{G12D}-mediated PanIN progression are likely not through altered UPR signaling. Combined, these results suggest that the absence of ATF3 in the presence of KRAS^{G12D} reduces the activation of factors promoting ADM and PanIN formation. Therefore, while the requirement of ATF3 for ADM can be bypassed by KRAS^{G12D}, ATF3 appears to be required for maintaining high-grade PanIN lesions.

An absence of *ATF3* affects the fibrotic and inflammatory pathways affected by oncogenic KRAS

Previous analysis of ATF3 in other cancers suggests an important role in fibrosis and inflammatory processes. To determine if the global absence of ATF3 affects these two elements in PDAC progression, we compared expression of markers for stellate cells and inflammation between *APK* and *Ptf1a*$^{creERT/+}$*Kras*$^{G12D/+}$ mice. Fibrosis, as determined by Masson's trichrome stain, was significantly higher 2 weeks post injury in *APK* tissue compared to *Ptf1a*$^{creERT/+}$ *Kras*$^{G12D/+}$ tissue (Fig. 7A, C), suggesting accelerated fibrosis in the absence of ATF3. By 5 weeks, no difference was observed in fibrosis between these two genotypes (Fig. 7B, D) as the level of fibrosis appears to lessen in *APK* mice. The increase in fibrosis was confirmed by picrosirius red staining (Fig. 7E). While *APK* pancreata are smaller and PanIN lesions do not progress to PDAC, there is still significant mucin accumulation based on PAS staining (Fig. 7F). Interestingly, analysis of α-smooth muscle actin, a marker of activated fibroblast cells, showed no difference in accumulation based on western blot analysis (Supplementary Fig. S11).

Next, to compare the immune cell infiltrate between *APK* and *Ptf1a*$^{creERT/+}$*Kras*$^{G12D/+}$ mice, we performed mass cytometry (CyTOF) on pancreatic tissue from mice 2 weeks after cerulein treatment. CyTOF experiments revealed a decreased infiltration of macrophages in *APK* mice with a concomitant increase in T lymphocyte accumulation (Fig. 8A, B). To confirm these findings, we performed IF for F4/80, a macrophage-specific marker (Fig. 8C). In confirmation of the CyTOF experiments, significantly fewer macrophages were observed in *APK* tissue compared to *Ptf1a*$^{creERT/+}$*Kras*$^{LSL\text{-}G12D/+}$ tissue 5 weeks after injury (Fig. 8D). These results suggest that the global loss of ATF3 has both acinar and non-acinar-specific role in affecting KRAS^{G12D}-mediated PDAC progression.

Discussion

In this study, we identified a novel role for ATF3 in recurrent pancreatic injury and progression to PDAC. Recurrent pancreatitis is a significant risk factor for PDAC, possibly due to the combined effects of inflammation and loss of the acinar cell phenotype through ADM. Through examining the effects of *Atf3* deletion on the acinar cell response to recurrent injury or constitutive KRAS activation, we identified a complex role for ATF3 in affecting multiple cell types within the pancreas. The absence of ATF3 prevented activation of key regulators of the ADM process and limited spontaneous PanIN formation in the presence of oncogenic KRAS. This requirement for ATF3 in ADM and PanIN progression appears dispensable when constitutive KRAS activation is combined with injury. However, the maintenance of high-grade PanINs and progression to PDAC still required ATF3. In addition, we observed a transient increase in fibrosis and an altered inflammatory response with a decreased macrophage infiltration. These results suggest that, in addition to ADM, ATF3 also affects stellate cells and myeloid cells. Whether this is through cell autonomous pathways or mediated by epithelial cell interactions needs to be investigated in future studies.

Previous work from our lab identified a requirement for ATF3 in activating ADM transcriptional profile during acute injury. We have now assessed ATF3's role in conditions

that promote PDAC. As observed in acute injury, ATF3 is required for changing the expression of key transcriptional regulators of the ADM process, including PDX1, SOX9, and MIST1. Increased expression of SOX9 and PDX1 observed during injury [42] is required for maintaining ADM morphology and expression of duct-specific genes such as *Ck19* [43]. Conversely, MIST1 expression is rapidly decreased. In the absence of ATF3, SOX9 and PDX1 expression are reduced compared to WT mice, while MIST1 expression was not completely repressed. The incomplete activation of the ADM transcriptome likely accounted for the more rapid regeneration exhibited by $Atf3^{-/-}$ mice following rCIP. Interestingly, structures resembling ADM were still observed and amylase accumulation was almost completely lost even while some MIST1 expression persisted. Therefore, recurrent injury still promoted the loss of mature acinar cell phenotype in the absence of ATF3, even without activation of SOX9. Similar observations of partial ADM have been observed in *Sox9*-deficient acinar cells in other studies [44], and was attributed to compensatory mechanisms involving hepatocyte nuclear factor 6 (HNF6 [45]). HNF6 works synergistically with SOX9 to promote ADM development.

Based on the rapid regeneration and reduced ADM exhibited by $Atf3^{-/-}$ mice, as well as the finding that *APK* mice do not develop PDAC, it is tempting to suggest that ATF3 may be a target for inhibiting KRAS-mediated PDAC. In fact, we observed little to no transformation of acinar cells following activation of $KRAS^{G12D}$ in mature *APK* acinar cells. Conversely, high-grade PanINs were readily observed in a subset of $Ptf1a^{creERT/+}Kras^{LSL\text{-}G12D/+}$ mice 13 weeks after $KRAS^{G12D}$ activation. However, our findings suggest that the absence of ATF3 is detrimental to regeneration when oncogenic KRAS is expressed in addition to injury. Following induction of pancreatitis, acinar cells expressing $KRAS^{G12D}$ appear to bypass the requirement of ATF3. SOX9 expression increases relative to non-CIP-treated mice and high-grade PanIN lesions are observed in *APK* mice 2 weeks following injury. However, SOX9 accumulation was reduced in *APK* mice compared to $Ptf1a^{creERT/+}Kras^{LSL\text{-}G12D/+}$ mice 2 weeks following injury and almost completely absent by 5 weeks suggesting an altered molecular profile for ADM and PanINs in the absence of ATF3. Unlike SOX9, other studies show that the expression of *Hnf6* is not maintained in more progressive lesions (PanIN lesions [45]). While we have not examined HNF6 expression in this study, it could explain the inability of *APK* tissue to progress to PDAC. These findings support histological findings that indicate a reduction in high-grade lesions in *APK* tissue.

While these findings support ATF3 requirement for persistent ADM, unlike in rCIP, the pancreata in *APK* mice did not regenerate. *APK* pancreata were significantly smaller in size than all other genotypes and histological analysis revealed increased fibrosis in *APK* tissue at 2 weeks, suggesting *Atf3*'s deletion affects stellate cell function. Whether the fibrosis observed in *APK* tissue limits pancreatic regeneration in these mice is unclear, but the amount and type of fibrosis can affect progression to PDAC. There is also a loss of fibrosis between 2 and 5 weeks in *APK* mice. While it is likely that this results from a general wasting within *APK* mice, we cannot rule out the possibility that factors are promoting resorption of the ECM. Therefore, future work will assess the ECM to determine if stellate cells in *APK* mice have a different expression profile. We also observed significant weight loss in *APK* mice relative to all other genotypes. *APK* mice lost on average 15% of their

starting body weight within 5 weeks of initiating cerulein-induce injury. This dramatic loss of weight could reflect pancreatic insufficiency due to the loss of pancreatic tissue in *APK* mice. However, a similar loss of pancreatic tissue also occurs in *Ptf1a*$^{creERT/+}$ *Kras*$^{LSL\text{-}G12D/+}$ mice, which do not show the same decrease in body weight. It is possible that *APK* mice develop cachexia, which can result in part from an altered metabolic phenotype, leading to significant loss of muscle. While ATF3 has not yet been implicated in metabolism, the related protein ATF4 does regulate amino acid metabolism in CD4+ T cells. Our previous work showed that ATF3-targeted many genes also regulated by ATF4 and Gene Ontology analysis identified dysregulation of several pathways involved in amino acid metabolism in *Atf3*$^{-/-}$ mice in response to acute pancreatic injury [22]. In support of a role for ATF3 in the inflammatory response during PDAC, we observe decreased myeloid cell infiltration combined with a trend in increased CD4+ T cells. Whether the gene expression/function of these cells is altered needs to be assessed.

Ultimately, this study was limited by the use of a germline deletion of *Atf3*. We chose to use these mice as they show no phenotype without the induction of some form of stress. However, we cannot determine whether the phenotypes are the result of acinar or non-acinar requirements for ATF3 gene regulation. We previously showed ATF3 enrichment at ~35% of the genes altered 4 h into cerulein-induced pancreatic injury including genes involved in affecting metabolism, promoting inflammation and ECM production. Therefore, it is possible that ATF3 regulates stellate and inflammatory cells indirectly through cross-talk with acinar cells. Lineage tracing analysis confirmed recombination, and therefore KRAS^{G12D} expression was limited to acinar cells and PanIN lesions derived from acinar cells. Therefore, we are not observing the results of activating KRAS in non-acinar cells. It is known that ATF3 can affect cancer progression in other systems through non-cell autonomous regulation [46–48]. However, these studies identified a non-cell autonomous for non-tumor cells expressing ATF3. Published data identified ATF3 expression in both inflammatory and ECM-producing cells in other pathologies including breast and lung cancer [29, 49] and our findings show that ATF3 is expressed in these cell populations in the context of PDAC. Therefore, it is likely that ATF3 directly affects the function of both stellate and myeloid cells in the context of PDAC. Indeed, it is possible that the transient increase in fibrosis and inability to maintain high-grade lesions in *APK* mice may be due to the difference in inflammatory response. Tumor-associated macrophages promote cancer fibrosis by secreting factors that activate fibroblast-mediated ECM remodeling [50].

In summary, the findings in this study support several roles for ATF3 in pancreatic injury and PDAC related to acinar, stellate, and immune cells. Future work to tease out cell-specific roles for ATF3 will need to involve cell-specific deletion of *Atf3* in the context of oncogenic KRAS. In addition, the potential for targeting the UPR, and ATF3 specifically, in the context of pancreatic pathologies will need to account for this multifaceted role.

Materials and methods

Mouse models

Two- to four-month-old male and female C57/Bl6 mice or congenic mice carrying a germline deletion of *Atf3* (*Atf3*$^{-/-}$ [51]) were used for rCIP studies. Alternatively, *Atf3*$^{-/-}$

mice were bred to mice in which a tamoxifen-inducible *cre* recombinase (*creERT*) was targeted to the *Ptf1a* allele ($Ptf1a^{creERT/+}$ [41]). $Atf3^{-/-}Ptf1a^{creERT/+}$ mice were crossed to mice carrying a constitutively active *Kras* gene ($KRAS^{G12D}$) preceded by *loxP* sites flanking a stop codon (*loxP-stop-loxP*; *LSL*) and targeted to the *Kras* allele ($Kras^{LSL\text{-}G12D/+}$ [52]). Through subsequent mating on a C57/Bl6 background, we generated $Atf3^{+/+}Ptf1a^{creERT/+}Kras^{LSL\text{-}G12D/+}$ (referred to as $Ptf1a^{creERT/+}Kras^{LSL\text{-}G12D/+}$) and $Atf3^{-/-}Ptf1a^{creERT/+}Kras^{LSL\text{-}G12D/+}$ mice (referred to as *APK*). In some cases, mice heterozygous for *Atf3* ($Atf3^{+/-}$) were included in the $Ptf1a^{creERT/+}Kras^{LSL\text{-}G12D/+}$ cohort as loss of a single copy of *Atf3* has no documented effects [22]. To allow lineage tracing of acinar cells, $Ptf1a^{creERT/+}$ $Kras^{LSL\text{-}G12D/+}$ and *APK* mice were mated to mice containing a *YFP* gene downstream of a *LSL* cassette targeted to the *Rosa26r* ($Rosa26r^{LSL\text{-}YFP/+}$) allele. Genotypes were confirmed before and after experimentation using the primers indicated in Supplementary Table S1.

Cerulein-induced pancreatitis

Mice were given normal chow and water ad libitum throughout the experiment. To induce recurrent pancreatic injury, $Atf3^{-/-}$ and $Atf3^{+/+}$ mice received intraperitoneal injections of cerulein (250 μg/kg body weight; Sigma; Cat. #17650–98-5; St. Louis, MO) or 0.9% saline (control) twice daily (9:00 h and 15:00 h) for 14 days (Supplementary Fig. S1). Mice were weighed daily to determine changes in body weight. Mice were killed 4 or 72 h after initial cerulein injection, or 1 or 7 days after the last cerulein injections. Pancreatic weight (g) was determined post mortem and compared to total body weight. For pancreatitis experiments, serum was obtained via cardiac puncture and assessed as described previously [21]. For experiments involving $KRAS^{G12D}$, $Atf3^{+/+}Ptf1a^{creERT/+}$ (designated as $Ptf1a^{creERT/+}$), $Atf3^{-/-}Ptf1a^{creERT/+}$, $Ptf1a^{creERT/+}$ $Kras^{LSL\text{-}G12D/+}$, and *APK* mice received 5 mg of tamoxifen (Sigma-Aldrich; Cat. #10540-29-1) each day for 5 days via oral gavage, producing cre-recombination efficiency ~95% (Supplementary Fig. S5). Seven days following tamoxifen treatment, cerulein (50 μg/kg) was administered via IP injection; eight times over 7 h (*n* values are indicated in each figure). Mice were weighed daily to monitor overall health and sacrificed if their body weight was 15% lower than their starting weight. Mice were killed 2 or 5 weeks after cerulein administration and pancreatic tissue collected and weighed.

Tissue fixation and histology

For histological analysis, pancreatic tissue was isolated from the head and tail of the pancreas and processed as described [22]. To assess overall histology and identify differences in pancreatic tissue architecture, sections were stained with H&E. To assess fibrosis, paraffin sections were stained using Masson's Trichrome stain (ab150686; Abcam Inc.) or Picrosirius Red (Polysciences, Inc.; Catalog #24901-500) and fibrosis quantified using ImageJ as a percent of total tissue area. Mucin accumulation was visualized using an Alcian Blue stain kit (ab150662; Abcam Inc.) and staining quantified as a percentage of the whole tissue area. Periodic-acid Schiff staining was also performed (Sigma-Aldrich Kit; Catalog# 3951and 3952) and quantified by scoring PanIN lesions as PAS+ (>50%), partially PAS+ (<50%), or PAS negative. Lesions were scored over at least three sections from both the duodenal and splenic regions of the pancreas.

Tissue sections were scored for ADM, PanINs, and PDAC by a pathologist blinded to genotype. Progressive lesions (PanINs) were graded based on nuclear irregularities, mucinous epithelium, and dense areas of fibrosis and inflammation surrounding PanIN lesions. In all cases, 10–15 images were taken for each sample and from multiple sections at least 200 μm apart using an Aperio CS2 Digital Scanner and Aperio ImageScope software (Leica Biosystems Imaging Inc, San Diego, CA, USA) and Leica Microscope DM5500B (Leica Microsystems, Wetzlar, Germany) with LAS V4.4 software.

To assess recombination efficiency through YFP detection, tissue was fixed in 4% methanol-free paraformaldehyde for 2 h and incubated at 4 °C. Post fixation, samples were incubated in 30% sucrose overnight at 4 °C, embedded in cryomatrix (Thermo Fisher Scientific), and sectioned to 6 μm using a Shandon cryostat (Thermo Fisher Scientific). YFP expression was determined natively without the use of immunostaining. The percent of YFP+ cells was determined by calculating the number of acinar cells positive for YFP over the total number of acinar cells ($n = 3$). A total of 8–10 images per tissue were obtained with a Leica Microscope DM5500B DFC365 FX camera for analysis.

Immunohistochemistry and immunofluorescence

IHC was performed on paraffin sections as described [22]. Following antigen retrieval, sections were permeabilized with 0.2% Triton-X in PBS, rinsed, then blocked in 5% sheep serum in PBS for 1 h at room temperature. Primary antibodies were diluted in 5% sheep serum in PBS and incubated overnight at 4 °C. Primary antibodies included rabbit α-PDX1 (1:1000; Abcam Inc. Cambridge, MA), rabbit α-amylase (1:600; Abcam Inc.), mouse α-CK19 (1:500; Abcam Inc.), p-ERK (1:50; Cell Signaling Technology, Danvers, MA), ATF3 (1:500; Cat#18665S, Cell Signaling Technology), and rabbit α-MIST1 (1:500 [53]). Sections were washed, then incubated in biotinylated mouse α-rabbit IgG secondary antibody (1:1000 dilution in 5% sheep serum) for 30 min at room temperature. Finally, sections were incubated in AB reagent for 30 min at room temperature and visualized using ImmPACT DAB Peroxidase (HRP) substrate (Vector Laboratories, Cat. #PK-4001/SK-4105). Slides were counterstained with hematoxylin and imaged using Leica Microscope DM5500B (Leica Microsystems) and LAS V4.4 software.

IF analysis was performed on paraffin-embedded tissue sections similar to IHC with the exception of quenching with hydrogen peroxidase. Primary antibodies used included rabbit α-SOX9 (1:250; Millipore Sigma), rabbit α-Ki67 (1:250; Abcam Inc.), and rat α-F4/80 (1:200; Abcam Inc.). After washing, slides were incubated in α-rabbit (or rat) IgG conjugated to TRITC (1:300; Jackson ImmunoResearch, West Grove, PA) or FITC (1:300; Jackson ImmunoResearch) diluted in 5% sheep serum in PBS. Prior to mounting in Vectashield Permafluor mountant (Thermo Fisher Scientific), sections were incubated in DAPI (diluted 1:1000 in PBS; Thermo Fisher Scientific). Staining was visualized using Leica DFC365 FX camera on the Leica DM5500B microscope. Images were taken on Leica LAS V4.4 software.

Protein isolation and immunoblots

For whole tissue protein, pancreatic tissue was taken from the middle portion of the pancreas and flash frozen in liquid nitrogen. Samples were processed as described (Young et al. (2018)). Either 2 μg (amylase) or 40 μg of protein (SOX9, p-ERK, BiP/GRP78, CHOP, ATF4, and αSMA) were resolved by 12% SDS-PAGE and transferred to a PVDF membrane. Western blotting was performed as described [54]. For primary antibodies against p-ERK (diluted 1:500) and total ERK (t-ERK; diluted 1:500; Cell Signaling Technology), antibodies were diluted in 0.1% TBST with 5% BSA. All other primary antibodies were diluted in 5% NFDM overnight at 4 °C. Rabbit primary antibodies included α-amylase (1;1000), α-SOX9 (1:500), α-CHOP (1:1500; Cell Signaling #2895), α-BiP/GRP78 (1:1000; Cell Signaling #3177), α-ATF4 (1:1000; Cell Signaling #11815), and αSMA (1:500). Secondary antibody α-rabbit HRP was diluted 1:10,000 in 5% NFDM (Jackson Labs). Blots were incubated 1 h at room temperature, washed, then incubated in Western ECL (Bio-Rad) substrate before being imaged on a VersaDoc system with Quantity One analysis software (Bio-Rad). Protein was quantified using densitometry on ImageJ and normalized to t-ERK accumulation.

RNA isolation and RNA-seq

Total RNA was isolated from whole pancreatic tissue 4 and 72 h after induction of CIP in WT and $Atf3^{-/-}$ mice. qRT-PCR was performed as previously described [22] using primers for *Mek* and *Egfr*. These values were normalized to *Mrpl* expression as previously described [22]. Primers include:

Mek: 5’ GGGGAACTGAAGGATGA 3’ 5’GGAGTTGC ACTCGTGCAGTA 3’

Egfr: 5’ CTGCCAAGGCACAAGTAACA 3’ 5’ GTTG AGGGCAATGAGGACAT 3’

Egfr: 5’ CTGCCAAGGCACAAGTAACA 3’ 5’ GTTG AGGGCAATGAGGACAT 3’

Single-cell RNA-seq was performed on tumors derived from orthotopic transplantation of 50,000 KPC ($Ptf1a^{+/cre}$; $p53^{+/R172H}$;$KRAS^{LSL\text{-}G12D}$) tumor cells 17 days after transplantation into 19-week-old syngeneic *BL6j* mice. Tumors were dissociated to single cells using enzymatic digestion and run through the 10X scRNA genomics platform. Cells were clustered based on known cell-specific markers. A full description of this work is available in Steele et al. [55] and Kemp et al. (under revision).

CyTOF—mass cytometry

CyTOF was carried out using Fluidigm reagents (Fluidigm Corporation; San Francisco, CA) unless otherwise noted. Whole pancreas tissue was digested with agitation in 1 mg/mL collagenase type V (Sigma) for 15 min at 37 °C in RPMI buffer. Cell and tissue fragment mixtures were filtered sequentially through 100 and 40 micron filters and washed in ice-cold Maxpar PBS. Single cells were subjected to the Cell ID Cisplatin^{ID} reagent (1:2000 dilution) for 5 min at room temperature to identify live cells at the time of analysis. Samples were then stained with a panel of surface antibodies (Supplementary Table S2) for 30 min at room temperature according to the manufacturer’s instructions. Cells were washed in cell staining buffer twice before cell fixation with 1.6% methanol-free formaldehyde (Thermo Fisher) for

10 min at room temperature. Samples were transferred into Nuclear Antigen Staining Buffer for 20 min at room temperature, then washed twice with Nuclear Antigen Staining Perm prior to intracellular staining. Intracellular antibodies were incubated with cells for 45 min at room temperature. Cells were then washed twice with Nuclear Antigen Staining Perm, and twice with cell staining buffer. Lastly, cells were resuspended in 1:2000 Intercalator solution in Fix and Perm buffer. Samples were acquired at the University of Rochester's (New York, NY) CyTOF2 facility in accordance with the manufacturer's protocol.

Sample size and statistical analysis

All animal experiments were performed at least two times (different days) with an n value >3. The numbers of animals used were based on the obtaining significance offset by the ethical use of animals within the study. No randomization of the animals was performed and no examples were excluded from this study. In some cases, mice needed to be sacrificed if they lost >15% of the starting weight as indicated by local our Animal Care Committee. In most cases, significance could be obtained from cohorts with five animals. Data were analyzed using either Student's t-test (unpaired, two-tailed), one-way ANOVA, or two-way ANOVA with Tukey's post-hoc test on GraphPad Prism 6 software. Repeated measures two-way ANOVA with Tukey's post-hoc test was used for weight loss over time. In all cases, data are shown with individual samples and error bars representing the mean ± standard error (SE). P value <0.05 was considered significant.

Supplementary Material

Refer to Web version on PubMed Central for supplementary material.

Acknowledgements

The authors wish to acknowledge the ongoing support of several national research funding agencies for this work including the Canadian Institutes of Health Research (MOP#PJT166029), the Cancer Research Society of Canada, and the Rob Lutterman Foundation for Pancreatic Cancer Research. This work would not be possible without specific support from a London Regional Cancer Centre Catalyst Grant, co-supported by Keith Sammit and an internal bridge grant from the University of Western Ontario. NA and JT were funded by studentships from the Ontario Graduate Scholarships and Cancer Research and Technology Training (CaRTT) program. MFK was supported by an NSERC summer studentship. JS was supported by National Cancer Institute of the National Institutes of Health under award number K08CA234222.

References

1. Ron D, Walter P. Signal integration in the endoplasmic reticulum unfolded protein response. Nat Rev Mol Cell Biol. 2007; 8:519–29. [PubMed: 17565364]
2. Kadowaki H, Nishitoh H. Signaling pathways from the endoplasmic reticulum and their roles in disease. Genes (Basel). 2013;4:306–33. [PubMed: 24705207]
3. Yoshida H, Matsui T, Hosokawa N, Kaufman RJ, Nagata K, Mori K. A time-dependent phase shift in the mammalian unfolded protein response. Dev Cell. 2003;4:265–71. [PubMed: 12586069]
4. Chang YS, Jalgaonkar SP, Middleton JD, Hai T. Stress-inducible gene Atf3 in the noncancer host cells contributes to chemotherapy-exacerbated breast cancer metastasis. Proc Natl Acad Sci USA. 2017;114:E7159–68. [PubMed: 28784776]
5. Song X, Lu F, Liu RY, Lei Z, Zhao J, Zhou Q, et al. Association between the ATF3 gene and non-small cell lung cancer. Thorac Cancer. 2012;3:217–23. [PubMed: 28920309]

6. Hackl C, Lang SA, Moser C, Mori A, Fichtner-Feigl S, Hellerbrand C, et al. Activating transcription factor-3 (ATF3) functions as a tumor suppressor in colon cancer and is up-regulated upon heat-shock protein 90 (Hsp90) inhibition. BMC Cancer. 2010; 10:668. [PubMed: 21129190]
7. Yan F, Ying L, Li X, Qiao B, Meng Q, Yu L, et al. Overexpression of the transcription factor ATF3 with a regulatory molecular signature associates with the pathogenic development of colorectal cancer. Oncotarget. 2017;8:47020–36. [PubMed: 28402947]
8. Thakur PC, Miller-Ocuin JL, Nguyen K, Matsuda R, Singhi AD, Zeh HJ, et al. Inhibition of endoplasmic-reticulum-stress-mediated autophagy enhances the effectiveness of chemotherapeutics on pancreatic cancer. J Transl Med. 2018;16:190. [PubMed: 29986726]
9. Garcia-Carbonero N, Li W, Cabeza-Morales M, Martinez-Useros J, Garcia-Foncillas J. New hope for pancreatic ductal adenocarcinoma treatment targeting endoplasmic reticulum stress response: a systematic review. Int J Mol Sci. 2018;19:2468–2464.
10. Chien W, Ding LW, Sun QY, Torres-Fernandez LA, Tan SZ, Xiao J, et al. Selective inhibition of unfolded protein response induces apoptosis in pancreatic cancer cells. Oncotarget. 2014;5:4881–94. [PubMed: 24952679]
11. Hess DA, Humphrey SE, Ishibashi J, Damsz B, Lee AH, Glimcher LH, et al. Extensive pancreas regeneration following acinar-specific disruption of Xbp1 in mice. Gastroenterology. 2011;141:1463–72. [PubMed: 21704586]
12. Harding HP, Zhang Y, Ron D. Protein translation and folding are coupled by an endoplasmic-reticulum-resident kinase. Nature. 1999;397:271–4. [PubMed: 9930704]
13. Iwawaki T, Akai R, Kohno K. IRE1alpha disruption causes histological abnormality of exocrine tissues, increase of blood glucose level, and decrease of serum immunoglobulin level. PLoS ONE. 2010;5:e13052.
14. Li M, Baumeister P, Roy B, Phan T, Foti D, Luo S, et al. ATF6 as a transcription activator of the endoplasmic reticulum stress element: thapsigargin stress-induced changes and synergistic interactions with NF-Y and YY1. Mol Cell Biol. 2000; 20:5096–106. [PubMed: 10866666]
15. Bertolotti A, Zhang Y, Hendershot LM, Harding HP, Ron D. Dynamic interaction of BiP and ER stress transducers in the unfolded-protein response. Nat Cell Biol. 2000;2:326–32. [PubMed: 10854322]
16. Blais JD, Filipenko V, Bi M, Harding HP, Ron D, Koumenis C, et al. Activating transcription factor 4 is translationally regulated by hypoxic stress. Mol Cell Biol. 2004;24:7469–82. [PubMed: 15314157]
17. B'chir W, Maurin AC, Carraro V, Averous J, Jousse C, Muranishi Y, et al. The eIF2α/ATF4 pathway is essential for stress-induced autophagy gene expression. Nucleic Acids Res. 2013;41:7683–99. [PubMed: 23804767]
18. Pakos-Zebrucka K, Koryga I, Mnich K, Ljujic M, Samali A, Gorman AM. The integrated stress response. EMBO Rep. 2016; 17:1374–95. [PubMed: 27629041]
19. Jiang HY, Wek SA, McGrath BC, Lu D, Hai T, Harding HP, et al. Activating transcription factor 3 is integral to the eukaryotic initiation factor 2 kinase stress response. Mol Cell Biol. 2004; 24:1365–77. [PubMed: 14729979]
20. Iida K, Li Y, McGrath BC, Frank A, Cavener DR. PERK eIF2 alpha kinase is required to regulate the viability of the exocrine pancreas. BMC Cell Biol. 2007;8:38. [PubMed: 17727724]
21. Kowalik AS, Johnson CL, Chadi SA, Weston JY, Fazio EN, Pin CL. Mice lacking the transcription factor Mist1 exhibit an altered stress response and increased sensitivity to caerulein-induced pancreatitis. Am J Physiol Gastrointest Liver Physiol. 2007;292: G1123–1132. [PubMed: 17170023]
22. Fazio EN, Young CC, Toma J, Levy M, Berger KR, Johnson CL, et al. Activating transcription factor 3 promotes loss of the acinar cell phenotype in response to cerulein-induced pancreatitis in mice. Mol Biol Cell. 2017;28:2347–59. [PubMed: 28701342]
23. Kubisch CH, Logsdon CD. Secretagogues differentially activate endoplasmic reticulum stress responses in pancreatic acinar cells. Am J Physiol Gastrointest Liver Physiol. 2007;292:G1804–12. [PubMed: 17431218]

24. Kang Y, Chen CR, Massagué J. A self-enabling TGFbeta response coupled to stress signaling: Smad engages stress response factor ATF3 for Id1 repression in epithelial cells. Mol Cell. 2003;11:915–26. [PubMed: 12718878]
25. Je YJ, Choi DK, Sohn KC, Kim HR, Im M, Lee Y, et al. Inhibitory role of Id1 on TGF-β-induced collagen expression in human dermal fibroblasts. Biochem Biophys Res Commun. 2014;444:81–85. [PubMed: 24434151]
26. Gilchrist M, Thorsson V, Li B, Rust AG, Korb M, Roach JC, et al. Systems biology approaches identify ATF3 as a negative regulator of Toll-like receptor 4. Nature. 2006;441:173–8. [PubMed: 16688168]
27. Dawn B, Xuan YT, Guo Y, Rezazadeh A, Stein AB, Hunt G, et al. IL-6 plays an obligatory role in late preconditioning via JAK-STAT signaling and upregulation of iNOS and COX-2. Cardiovasc Res. 2004;64:61–71. [PubMed: 15364614]
28. Boespflug ND, Kumar S, McAlees JW, Phelan JD, Grimes HL, Hoebe K, et al. ATF3 is a novel regulator of mouse neutrophil migration. Blood. 2014;123:2084–93. [PubMed: 24470589]
29. Kim DE, Procopio MG, Ghosh S, Jo SH, Goruppi S, Magliozzi F, et al. Convergent roles of ATF3 and CSL in chromatin control of cancer-associated fibroblast activation. J Exp Med. 2017; 214:2349–68. [PubMed: 28684431]
30. Wu X, Nguyen BC, Dziunycz P, Chang S, Brooks Y, Lefort K, et al. Opposing roles for calcineurin and ATF3 in squamous skin cancer. Nature. 2010;465:368–72. [PubMed: 20485437]
31. Bandyopadhyay S, Wang Y, Zhan R, Pai SK, Watabe M, Iiizumi M, et al. The tumor metastasis suppressor gene Drg-1 downregulates the expression of activating transcription factor 3 in prostate cancer. Cancer Res. 2006;66:11983–90. [PubMed: 17178897]
32. Wang A, Arantes S, Yan L, Kiguchi K, McArthur MJ, Sahin A, et al. The transcription factor ATF3 acts as an oncogene in mouse mammary tumorigenesis. BMC Cancer. 2008;8:268. [PubMed: 18808719]
33. Song HM, Park GH, Eo HJ, Jeong JB. Naringenin-mediatedATF3 expression contributes to apoptosis in human colon cancer. Biomol Ther (Seoul). 2016;24:140–6. [PubMed: 26797111]
34. Kim KJ, Lee J, Park Y, Lee SH. ATF3 mediates anti-cancer activity of trans-10, cis-12-conjugated linoleic acid in human colon cancer cells. Biomol Ther (Seoul). 2015;23:134–40. [PubMed: 25767681]
35. Johnson CL, Kowalik AS, Rajakumar N, Pin CL. Mist1 is necessary for the establishment of granule organization in serous exocrine cells of the gastrointestinal tract. Mech Dev. 2004; 121:261–72. [PubMed: 15003629]
36. Tsuda M, Fukuda A, Roy N, Hiramatsu Y, Leonhardt L, Kakiuchi N, et al. The BRG1/SOX9 axis is critical for acinar cell-derived pancreatic tumorigenesis. J Clin Invest. 2018;128:3475–89. [PubMed: 30010625]
37. Shi G, Direnzo D, Qu C, Barney D, Miley D, Konieczny SF. Maintenance of acinar cell organization is critical to preventing Kras-induced acinar-ductal metaplasia. Oncogene. 2013;32:1950–8. [PubMed: 22665051]
38. Yadav D, Lowenfels AB. The epidemiology of pancreatitis and pancreatic cancer. Gastroenterology. 2013;144:1252–61. [PubMed: 23622135]
39. Kopp JL, Dubois CL, Schaffer AE, Hao E, Shih HP, Seymour PA, et al. Sox9+ ductal cells are multipotent progenitors throughout development but do not produce new endocrine cells in the normal or injured adult pancreas. Development. 2011;138:653–65. [PubMed: 21266405]
40. Pin CL, Rukstalis JM, Johnson C, Konieczny SF. The bHLH transcription factor Mist1 is required to maintain exocrine pancreas cell organization and acinar cell identity. J Cell Biol. 2001;155:519–30. [PubMed: 11696558]
41. Roy N, Takeuchi KK, Ruggeri JM, Bailey P, Chang D, Li J, et al. PDX1 dynamically regulates pancreatic ductal adenocarcinoma initiation and maintenance. Genes Dev. 2016;30:2669–83. [PubMed: 28087712]
42. Pinho AV, Rooman I, Reichert M, De Medts N, Bouwens L, Rustgi AK, et al. Adult pancreatic acinar cells dedifferentiate to an embryonic progenitor phenotype with concomitant activation of a senescence programme that is present in chronic pancreatitis. Gut. 2011;60:958–66. [PubMed: 21193456]

43. Carrière C, Young AL, Gunn JR, Longnecker DS, Korc M. Acute pancreatitis accelerates initiation and progression to pancreatic cancer in mice expressing oncogenic Kras in the nestin cell lineage. PLoS ONE. 2011;6:e27725.
44. Delous M, Yin C, Shin D, Ninov N, Debrito Carten J, Pan L, et al. Sox9b is a key regulator of pancreaticobiliary ductal system development. PLoS Genet. 2012;8:e1002754.
45. Prevot PP, Simion A, Grimont A, Colletti M, Khalaileh A, Van den Steen G, et al. Role of the ductal transcription factors HNF6 and Sox9 in pancreatic acinar-to-ductal metaplasia. Gut. 2012;61:1723–32. [PubMed: 22271799]
46. Gardian K, Janczewska S, Olszewski WL, Durlik M. Analysis of pancreatic cancer microenvironment: role of macrophage infiltrates and growth factors expression. J Cancer. 2012;3:285–91. [PubMed: 22773932]
47. Kurahara H, Shinchi H, Mataki Y, Maemura K, Noma H, Kubo F, et al. Significance of M2-polarized tumor-associated macrophage in pancreatic cancer. J Surg Res. 2011;167:e211–9. [PubMed: 19765725]
48. Helm O, Held-Feindt J, Grage-Griebenow E, Reiling N, Ungefroren H, Vogel I, et al. Tumor-associated macrophages exhibit pro- and anti-inflammatory properties by which they impact on pancreatic tumorigenesis. Int J Cancer. 2014;135:843–61. [PubMed: 24458546]
49. Mallano T, Palumbo-Zerr K, Zerr P, Ramming A, Zeller B, Beyer C, et al. Activating transcription factor 3 regulates canonical TGFβ signalling in systemic sclerosis. Ann Rheum Dis. 2016; 75:586–92. [PubMed: 25589515]
50. Clark CE, Hingorani SR, Mick R, Combs C, Tuveson DA, Vonderheide RH. Dynamics of the immune reaction to pancreatic cancer from inception to invasion. Cancer Res. 2007;67:9518–27. [PubMed: 17909062]
51. Harding HP, Zhang Y, Zeng H, Novoa I, Lu PD, Calfon M, et al. An integrated stress response regulates amino acid metabolism and resistance to oxidative stress. Mol Cell. 2003;11:619–33. [PubMed: 12667446]
52. Hingorani SR, Petricoin EF, Maitra A, Rajapakse V, King C, Jacobetz MA, et al. Preinvasive and invasive ductal pancreatic cancer and its early detection in the mouse. Cancer Cell. 2003;4:437–50. [PubMed: 14706336]
53. Pin CL, Bonvissuto AC, Konieczny SF. Mist1 expression is a common link among serous exocrine cells exhibiting regulated exocytosis. Anat Rec. 2000;259:157–67. [PubMed: 10820318]
54. Young CC, Baker RM, Howlett CJ, Hryciw T, Herman JE, Higgs D, et al. The loss of ATRX increases susceptibility to pancreatic injury and oncogenic KRAS in female but not male mice. Cell Mol Gastroenterol Hepatol. 2019;7:93–113. [PubMed: 30510993]
55. Steele NG, Biffi G, Kemp SB, Zhang Y, Drouillard D, Syu L. et al. Inhibition of Hedgehog signaling alters fibroblast composition in pancreatic cancer. Clin Canc Res. 2021;27:2023–37.

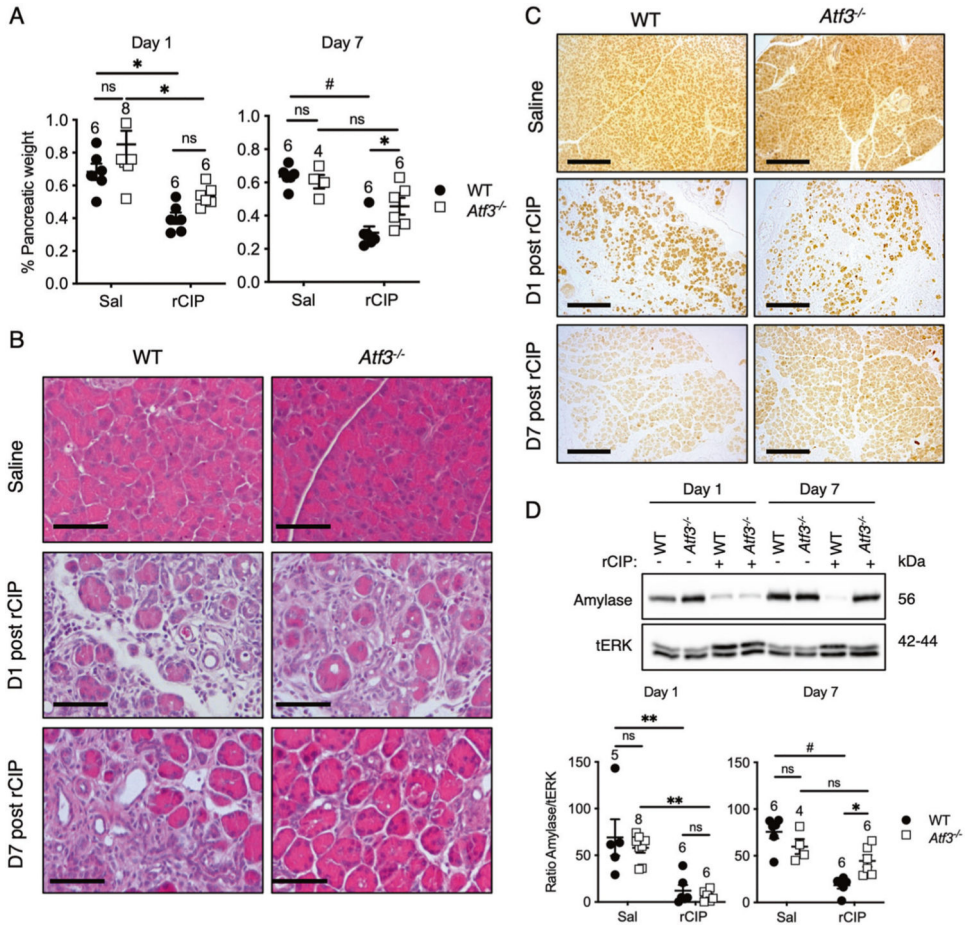

Fig. 1. *Atf3*$^{-/-}$ mice show accelerated pancreatic regeneration in response to recurrent pancreatic injury.

A Quantification of pancreatic weight as a % of body weight in mice treated with saline (Sal) or cerulein (rCIP) 1 and 7 days after cessation of treatment. Cerulein-treated wild-type (WT) and *Atf3*$^{-/-}$ mice showed significant decrease in pancreatic weight at day 1 (D1) with no significant difference between genotypes. Seven days into recovery, only cerulein-treated WT mice showed a decrease in pancreatic weight relative to other groups. **B** Representative H&E histology shows loss of acinar tissue and increased number of duct-like structures 1 day after rCIP in both genotypes. By day 7 after rCIP, there is reduced damage and increased acinar cell area in *Atf3*$^{-/-}$ tissue compared to WT tissue. Magnification bars = 100 μm. **C** Immunohistochemistry (IHC) for amylase in WT and *Atf3*$^{-/-}$ pancreatic tissue from mice treated with saline or 1 or 7 days following rCIP. Magnification bar = 400 μm. **D** Western blot analysis and quantification of amylase accumulation in pancreatic extracts from mice treated with saline (−) or rCIP (+). In all cases, ns is not significant; *$p < 0.05$, **$p < 0.01$, $^{\#}p < 0.001$; *N* values are indicated above the data points; error bars represent mean ± SEM. kDa kilodalton. To determine significance, a two-way ANOVA was performed with Tukey's post-hoc test.

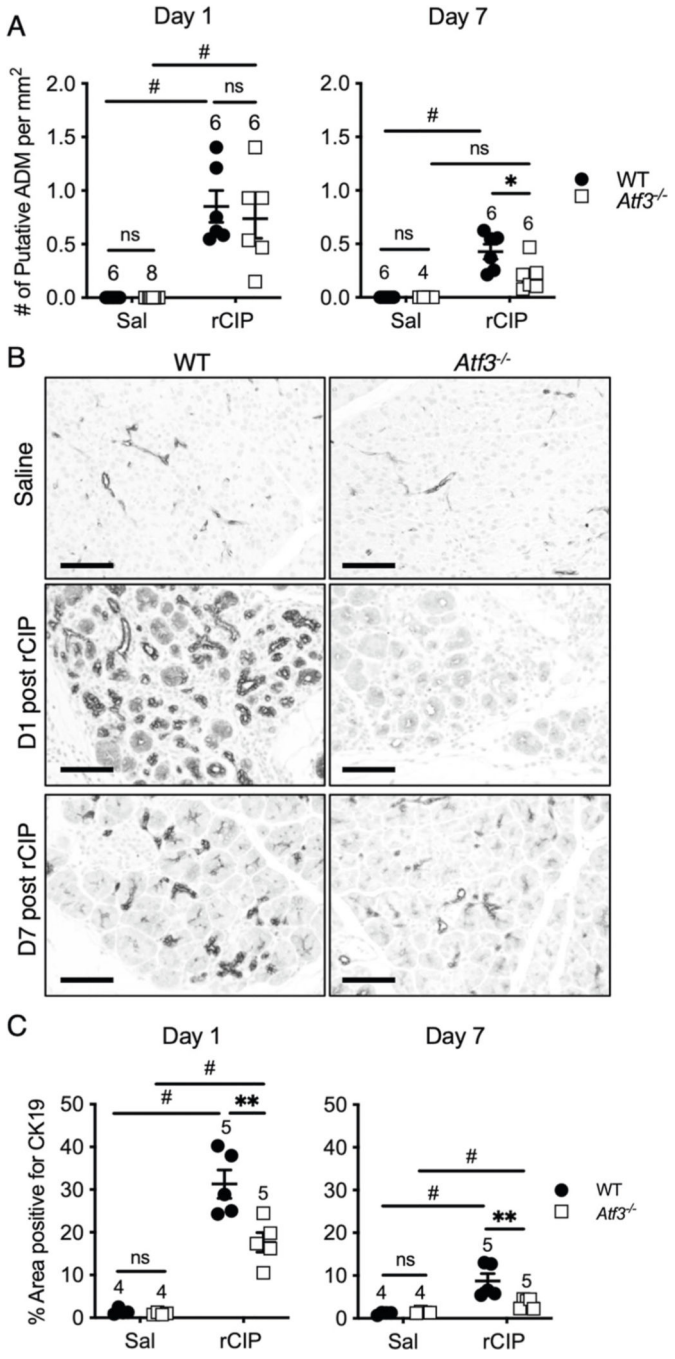

Fig. 2. *Atf3*$^{-/-}$ mice exhibit reduced ADM in response to recurrent pancreatic injury.

A Quantification of ADM-like structures following recurrent cerulein-induced pancreatitis (rCIP) based on H&E analysis. A significant increase in putative ADM structures was observed 1 day after rCIP in both genotypes, but no difference between genotypes in the rCIP cohorts. Seven days after rCIP treatment, significantly fewer putative ADM structures were observed in rCIP-treated *Atf3*$^{-/-}$ mice compared wild-type (WT). **B** Representative IHC for CK19 in WT and *Atf3*$^{-/-}$ pancreatic tissue following saline or rCIP. Magnification bars = 70 μm. **C** Quantification of CK19 IHC revealed decreased CK19 accumulation 1 and

7 days after rCIP in *Atf3*$^{-/-}$ mice relative to WT mice. In all cases, *N* values are indicated above the data points; ns not significant; *$p < 0.05$; **$p < 0.01$, $^{\#}p < 0.001$; error bars represent mean ± SEM. To determine significance, a two-way ANOVA was performed with Tukey's post-hoc test.

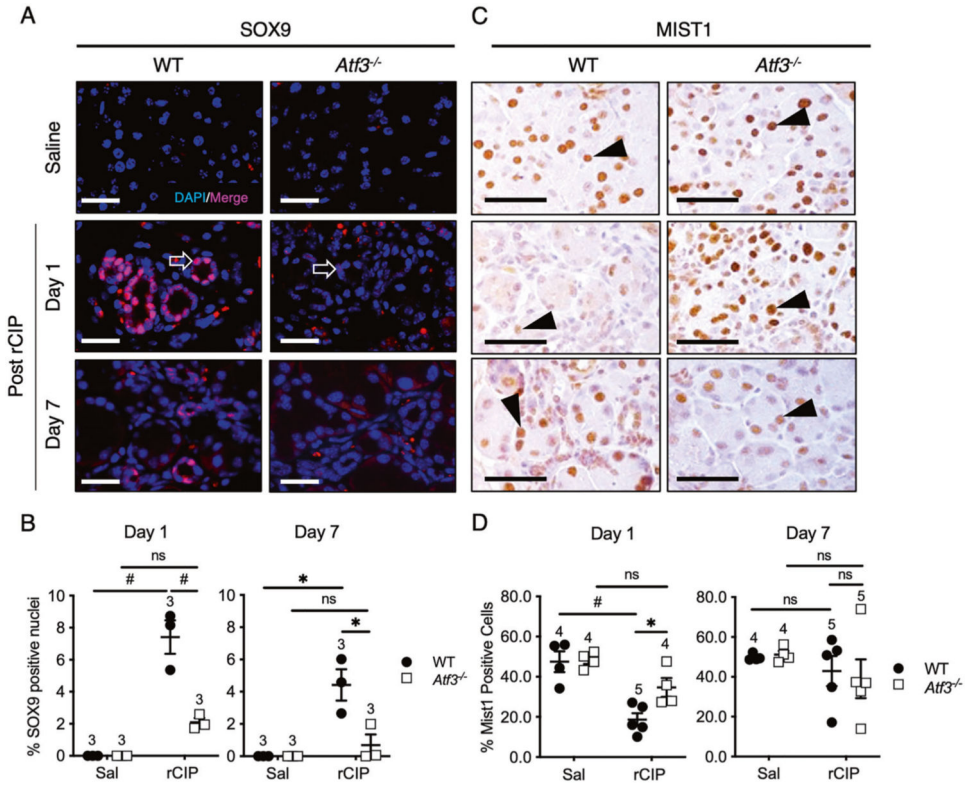

Fig. 3. The ADM transcriptional program is reduced in the absence of ATF3.

A Representative IF for SOX9 in WT and *Atf3*$^{-/-}$ pancreatic tissue from mice 1 or 7 days following saline or recurrent cerulein-induced pancreatitis (rCIP) treatment. Sections were counterstained with DAPI to reveal nuclei. Arrows indicate SOX9+ cells. Magnification bars = 20 μm. **B** Quantification of the percentage of SOX9+ nuclei showed that significantly fewer cells express SOX9 in *Atf3*$^{-/-}$ tissue at both time points. **C** Representative IHC for MIST1 in WT and *Atf3*$^{-/-}$ pancreatic tissue 1 or 7 days following saline or rCIP. Arrowheads indicate MIST1+ cells. Magnification bars = 50 μm. **D** Quantification of the percent MIST1+ nuclei confirmed that significantly more cells express MIST1 in *Atf3*$^{-/-}$ tissue. For graphs, *N* values are indicated above data points; ns not significant; $^{*}p < 0.05$, $^{\#}p < 0.001$; error bars represent mean ± SEM. To determine significance, a two-way ANOVA was performed with Tukey's post-hoc test.

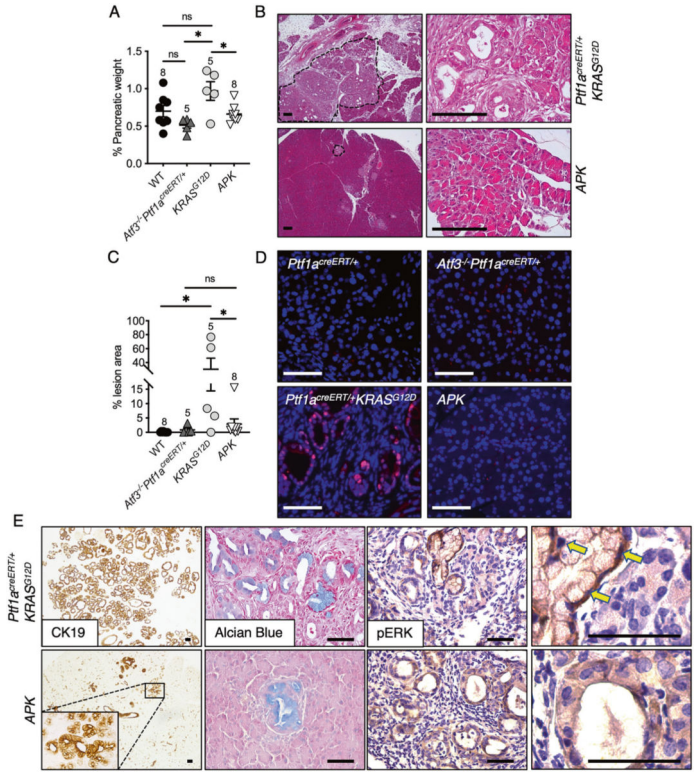

Fig. 4. *Atf3*$^{-/-}$ mice show minimal spontaneous ADM and PanIN formation following activation of oncogenic KRAS.

A Quantification of pancreatic weight as a % of body weight 13 weeks after activation of KRAS^{G12D} with tamoxifen. Pancreatic weight is increased in *Ptf1a*$^{creERT/+}$*Kras*$^{G12D/+}$ (indicated as KRAS^{G12D}) mice relative to *Ptf1a*$^{creERT/+}$, *Ptf1a*$^{creERT/+}$*Atf3*$^{-/-}$ and *APK* mice. **B** Low (left) and high (right) magnification of representative H&E on pancreatic tissue from *Ptf1a*$^{creERT/+}$*Kras*$^{G12D/+}$ and *APK* mice 13 weeks after KRAS^{G12D} activation. Extensive lesions were observed in 2/5 *Ptf1a*$^{creERT/+}$ *Kras*$^{G12D/+}$ mice but only minimal lesions were observed in *APK* tissue. Typical lesions are outlined. Magnification bars = 100 μm. **C** Quantification of lesion area based on H&E histology. Lesion area was increased in *Ptf1a*$^{creERT/+}$*Kras*$^{G12D/+}$ tissue relative to all other genotypes. For all graphs, *N* values are indicated above data points; ns not significant; *$p < 0.05$; error bars represent mean ± SEM. To determine significance, a one-way ANOVA was performed with Tukey's post-hoc test. **D** Representative IF for SOX9 (red) on pancreatic tissue for each genotype. Sections were counterstained with DAPI to reveal nuclei. Magnification bars = 60 μm. **E** Representative brightfield images of CK19 IHC, Alcian blue, and p-ERK IHC on pancreatic tissue from *Ptf1a*$^{creERT/+}$*Kras*$^{G12D/+}$ and *APK* mice. P-ERK IHC sections were counterstained with hematoxylin to reveal nuclei. Yellow arrows indicate nuclear staining. Magnification bars = 50 μm.

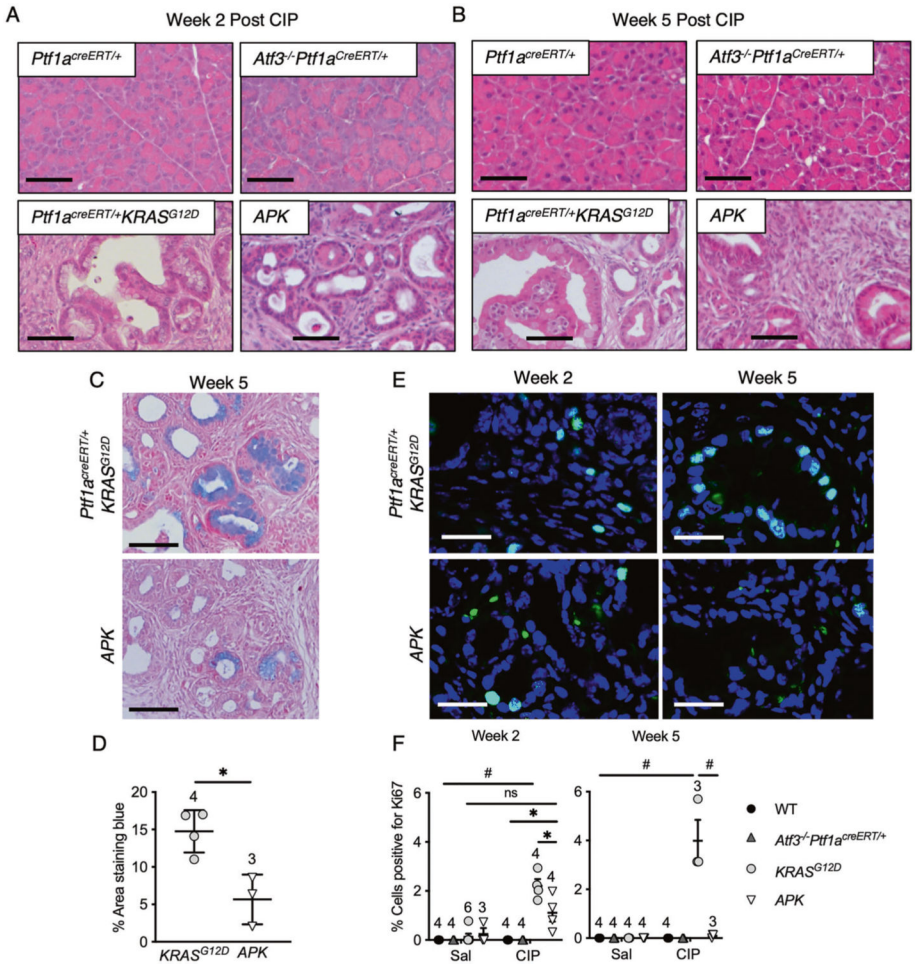

Fig. 5. ATF3 is dispensable for progression but not maintaining PanINs when KRAS^{G12D} activation is coupled with pancreatic injury.

Representative H&E histology on pancreatic tissue **A** 2 and **B** 5 weeks after cerulein treatment for all genotypes. No lesions were observed in *Ptf1a$^{creERT/+}$* or *Atf3$^{-/-}$Ptf1a$^{creERT/+}$* tissue. Extensive lesions and no acinar tissue were visible at either time point in both *Ptf1a$^{creERT/+}$Kras$^{G12D/+}$* and *APK* tissue following cerulein treatment. Magnification bars = 100 μm. **C** Representative Alcian blue histology on *Ptf1a$^{creERT/+}$Kras$^{G12D/+}$* and *APK* tissue following cerulein treatment showed significantly more alcian blue staining in *Ptf1a$^{creERT/+}$Kras$^{G12D/+}$* mice which is quantified in **D. E** Representative IF for Ki-67 in *Ptf1a$^{creERT/+}$Kras$^{G12D/+}$* and *APK* tissue 2 and 5 weeks following cerulein treatment. Magnification bar = 50 μm. **F** Quantification of the percentage of Ki-67+ cells indicated significantly fewer positive cells in *APK* tissue. For all graphs, *N* values are indicated in brackets or above data points; ns not significant; **p* <0.05, $^{\#}p <$ 0.001; error bars represent mean ± SEM. To determine significance, Student's *t*-test (**D**) or (**F**) two-way ANOVA was performed with Tukey's post-hoc test.

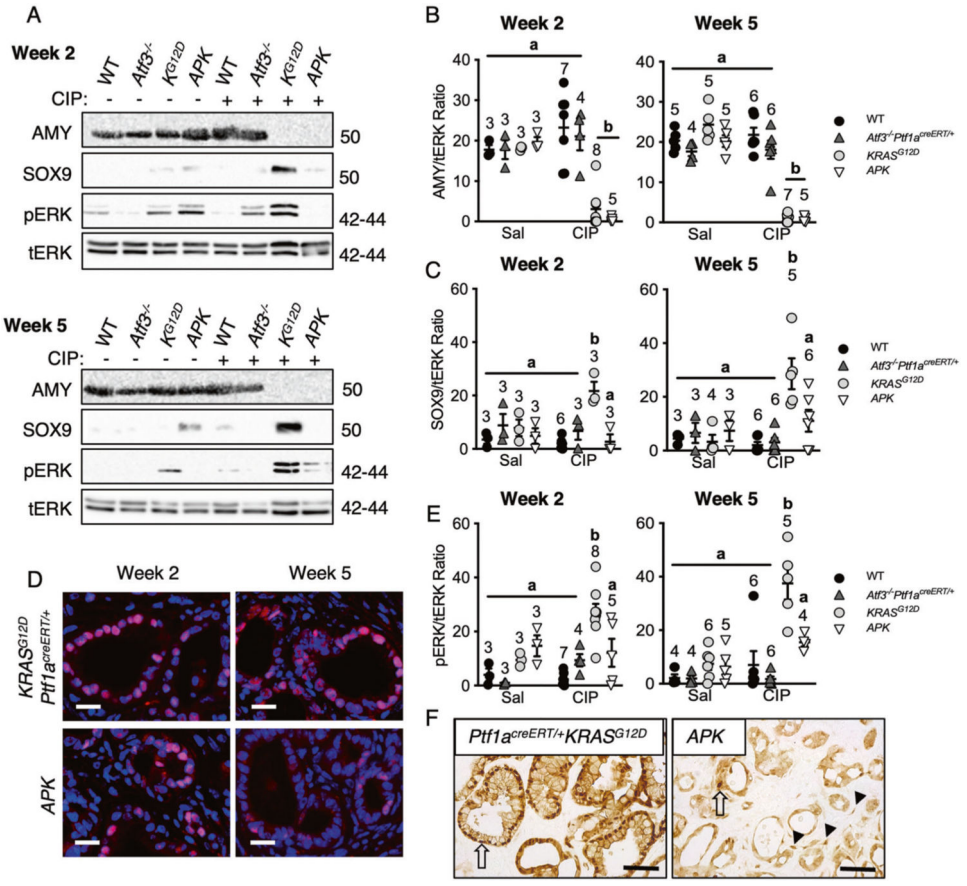

Fig. 6. ATF3 is required for establishment and maintenance of the molecular ADM profile in the presence of KRAS^{G12D}.

A Representative western blots for amylase (AMY), SOX9, phosphorylated ERK (p-ERK), and total ERK (t-ERK, loading control). No detectable amylase accumulation is observed in *Ptf1a*$^{creERT/+}$*Kras*$^{G12D/+}$ or *APK* tissue (quantified in **B**), while SOX9 and p-ERK accumulation increases only in *Ptf1a*$^{creERT/+}$*Kras*$^{G12D/+}$ tissue (quantified in **C** and **E**, respectively). Similar results are obtained both 2 and 5 weeks after cerulein (CIP) treatment. For all graphs, *N* values are indicated above data points; significantly different values are indicated by letters. In **C** and **E**, *Ptf1a*$^{creERT/+}$*Kras*$^{G12D/+}$ values are significantly different from all genotypes ($p < 0.001$) even from *APK* mice ($p < 0.05$). Error bars represent mean ± SEM. To determine significance, a two-way ANOVA was performed with Tukey's post-hoc test. **D** Representative IF for SOX9 (red) on pancreatic tissue from *Ptf1a*$^{creERT/+}$*Kras*$^{G12D/+}$ or *APK* mice. Sections were counterstained with DAPI to reveal nuclei. Magnification bars = 20 μm. **F** Representative images of p-ERK IHC stained pancreatic tissue from *Ptf1a*$^{creERT/+}$*Kras*$^{G12D/+}$ and *APK* mice 2 weeks after cerulein treatment. *Ptf1a*$^{creERT/+}$*Kras*$^{G12D/+}$ mice show predominant nuclear stain (arrows), while p-ERK is more diffuse in APK mice. In addition, some stromal p-ERK positive cells were observed (arrowheads). Magnification bars = 50 μm.

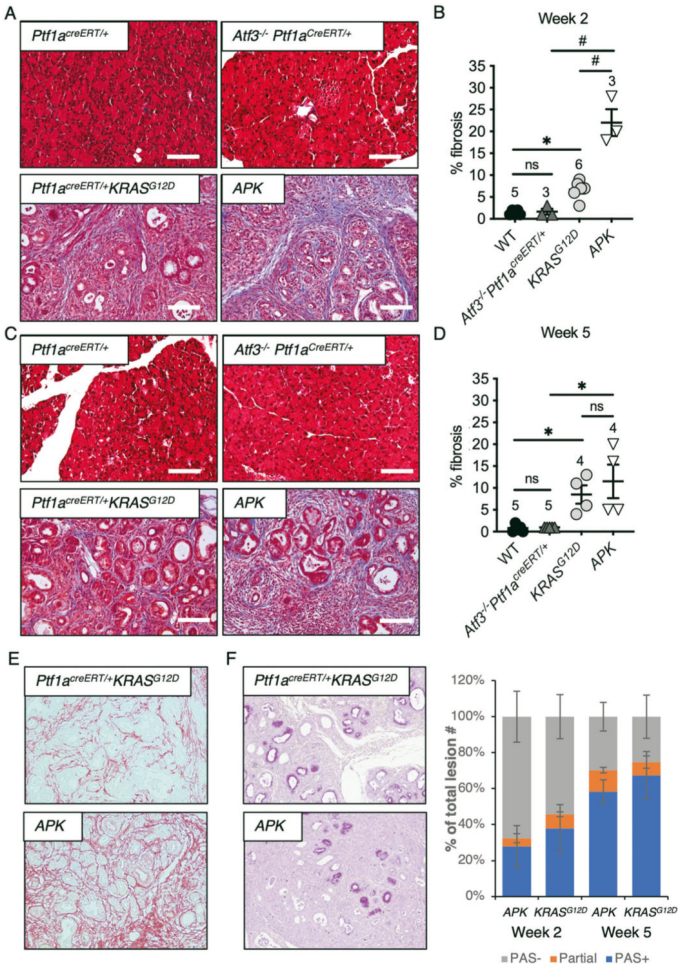

Fig. 7. *APK* mice display enhanced fibrosis at early time point after pancreatic injury.

Representative images of Masson trichrome staining **A** 2 or **C** 5 weeks after cerulein treatment in all genotypes. Magnification bars = 140 μm. **B, D** Quantification of fibrosis based on trichrome staining showed increased fibrosis in *APK* tissue compared to all other genotypes 2 weeks post CIP and increased fibrosis in $Ptf1a^{creERT/+}Kras^{G12D/+}$ and *APK* mice 5 weeks after cerulein treatment. *N* values are indicated above data points; ns not significant; $*p < 0.05$, $^{\#}p < 0.001$; error bars represent mean ± SEM. To determine significance, a one-way ANOVA was performed with Tukey's post-hoc test. Representative images of **E** Picrosirius Red or F Periodic-acid Schiff (PAS) staining 2 weeks after cerulein treatment in $Ptf1a^{creERT/+}$ $Kras^{G12D/+}$ and *APK* mice. Magnification bars = 140 μm. Quantification of mucin-expressing lesions was based on >50% (PAS+), <50% (partial PAS), or 0% staining within all lesions. While trends of decreased PAS are observed, these are not significant based on a two-way ANOVA test.

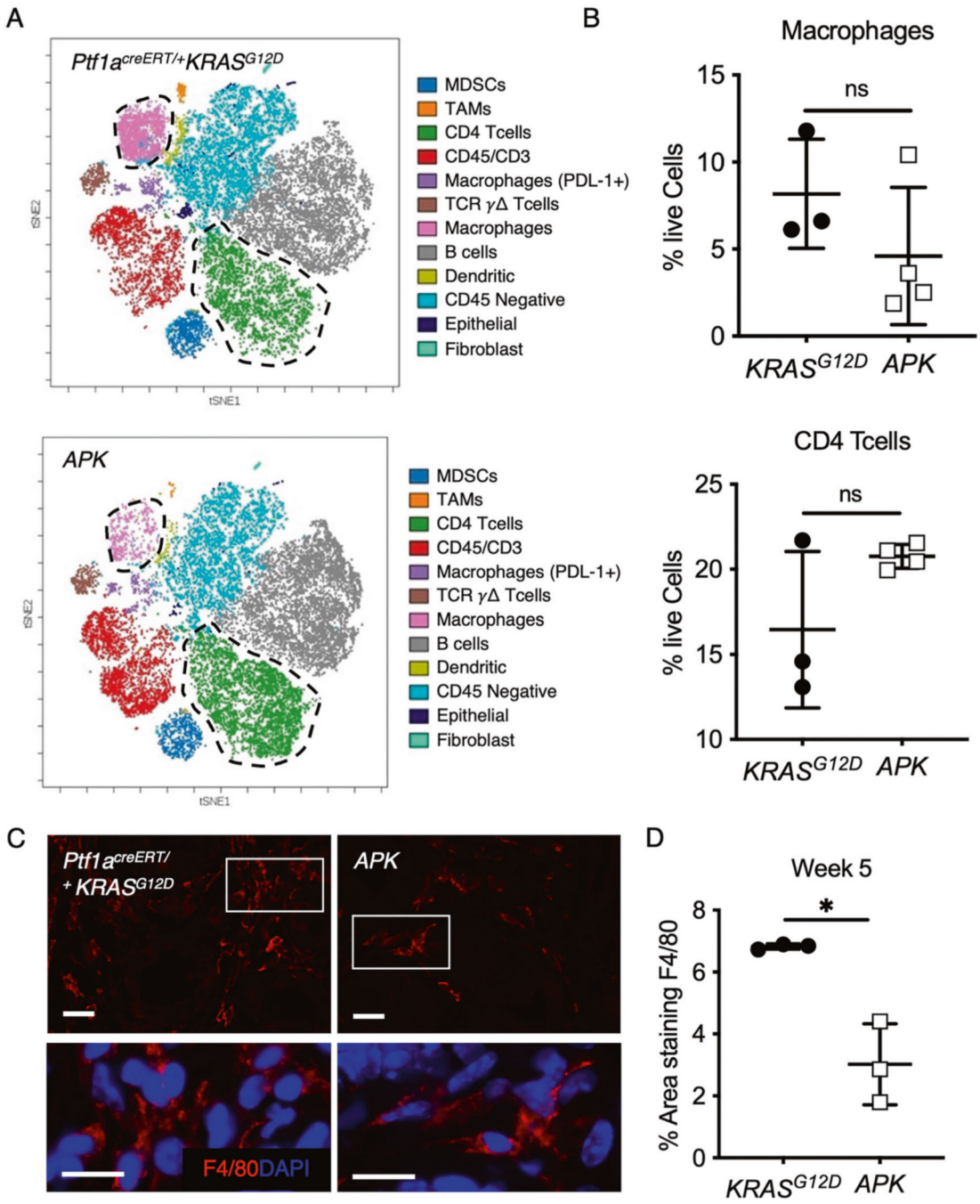

Fig. 8. APK mice showed an altered inflammatory response to pancreatic damage.

A Representative viSNE analysis performed on cytometric flow data obtained from *Ptf1a*$^{creERT/+}$*Kras*$^{G12D/+}$ (*KRAS*^{G12D}) and *APK* mice pancreata at 2 weeks post CIP (n = 3–4). **B** Quantification of macrophage and CD4 T cells based on viSNE analysis suggested decreased macrophage and increased T lymphocyte accumulation in *APK* pancreata relative to *Ptf1a*$^{creERT/+}$*Kras*$^{G12D/+}$. **C** Representative IF images show significant fewer macrophages in *APK* mice based on the percent area of F4/80 staining, which is quantified in (**D**). *p <

0.05, error bars represent % mean ± SEM; $N = 3$. To determine significance, Student's *t*-test was performed.

Table 1

Histological analysis of pancreatic lesions in response to saline or cerulein treatment[a].

	Ptf1a$^{creERT/+}$		*Atf3*$^{-/-}$*Ptf1a*$^{creERT/+}$		*Ptf1a*$^{creERT/+}$*KRAS*$^{G12D/+}$		*APK*	
	2 weeks	**5 weeks**	**2 weeks**	**5 weeks**	**2 weeks**	**5 weeks**	**2 weeks**	**5 weeks**
Saline								
Normal	4	2	3	2	1	0	1	1
ADM	0	1	0	0	0	0	1	0
PanIN1	0	0	0	0	2	2	1	1
PanIN2	0	0	0	0	0	1	0	1
PanIN3	0	0	0	0	0	0	0	0
PDAC	0	0	0	0	0	0	0	0
Total no. of mice	4	3	3	2	3	3	3	3
Cerulein								
Normal	0	2	2	0	0	0	0	0
ADM	2	0	0	1	0	0	0	0
PanIN1	0	0	1	0	0	0	2	1
PanIN2	0	0	0	0	2	2	0	5
PanIN3	0	0	0	0	9	4	4	2
PDAC	0	0	0	0	1	1	0	0
Total no. of mice	2	2	3	1	12	7	6	8

[a]Pancreatic tissue was scored for the highest grade lesion within the tissue. Numbers do not include three *Ptf1a*$^{creERT/+}$*KRAS*$^{G12D/+}$ and one *APK* mouse that needed to be sacrificed prior to the experimental end point. These numbers reflect analysis of at least three sections separated by 100 μm for each animal.

Oncogene. Author manuscript; available in PMC 2022 April 16.